

Planar Reflection-Aware Neural Radiance Fields

CHEN GAO, Meta, USA

YIPENG WANG, Meta, USA

CHANGIL KIM, Meta, USA

JIA-BIN HUANG, University of Maryland, USA

JOHANNES KOPF, Meta, USA

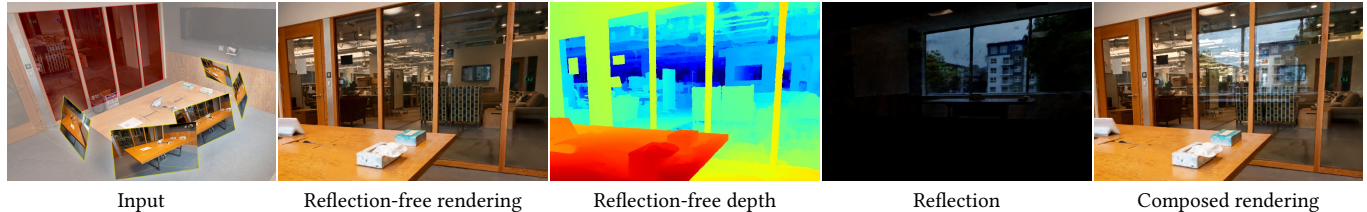


Fig. 1. **Planar reflection-aware novel view synthesis.** Our method takes multi-view capture data as input to jointly model planar reflectors and reconstruct radiance fields free of false geometries caused by reflections. This leads to accurate scene geometry, which benefits downstream applications, such as mesh extraction. Rendering along the primary ray results in a clean, reflection-free view, while explicitly rendering along the reflected ray allows us to reconstruct highly detailed reflections. By composing these two renderings, we achieve sharp and realistic novel view synthesis.

Neural Radiance Fields (NeRF) have demonstrated exceptional capabilities in reconstructing complex scenes with high fidelity. However, NeRF’s view dependency can only handle low-frequency reflections. It falls short when dealing with complex planar reflections, often interpreting them as erroneous scene geometries and leading to duplicated and inaccurate scene representations. To address this challenge, we introduce a planar reflection-aware NeRF that jointly models planar reflectors, such as windows, and explicitly casts reflected rays to capture the source of the high-frequency reflections. We query a single radiance field to render the primary color and the source of the reflection. We propose a sparse edge regularization to help utilize the true source of reflections for rendering planar reflections rather than creating a duplicate along the primary ray at the same depth. As a result, we obtain accurate scene geometry. Rendering along the primary ray results in a clean, reflection-free view, while explicitly rendering along the reflected ray allows us to reconstruct highly detailed reflections. Our extensive quantitative and qualitative evaluations of real-world datasets demonstrate our method’s performance in accurately handling reflections.

CCS Concepts: • **Computing methodologies** → **Computational photography**.

ACM Reference Format:

Chen Gao, Yipeng Wang, Changil Kim, Jia-Bin Huang, and Johannes Kopf. 2024. Planar Reflection-Aware Neural Radiance Fields. 1, 1 (November 2024), 9 pages. <https://doi.org/10.1145/nnnnnnn.nnnnnnn>

Authors’ addresses: Chen Gao, Meta, Seattle, Washington, USA, gaochen@meta.com; Yipeng Wang, Meta, Seattle, Washington, USA, yipeng.wang.99@outlook.com; Changil Kim, Meta, Seattle, Washington, USA, changil@meta.com; Jia-Bin Huang, University of Maryland, College Park, Maryland, USA, jbhuang@umd.edu; Johannes Kopf, Meta, Seattle, Washington, USA, jkopf@meta.com.

Permission to make digital or hard copies of all or part of this work for personal or classroom use is granted without fee provided that copies are not made or distributed for profit or commercial advantage and that copies bear this notice and the full citation on the first page. Copyrights for components of this work owned by others than ACM must be honored. Abstracting with credit is permitted. To copy otherwise, or republish, to post on servers or to redistribute to lists, requires prior specific permission and/or a fee. Request permissions from permissions@acm.org.

© 2024 Association for Computing Machinery.

XXXX-XXXX/2024/11-ART \$15.00

<https://doi.org/10.1145/nnnnnnn.nnnnnnn>

1 INTRODUCTION

Planar reflections are a ubiquitous and visually significant phenomenon in our everyday environments. Windows, in particular, are common planar reflectors, making their proper handling a critical aspect of realistic scene reconstruction. In this work, we focus on accurately modeling these planar reflections during scene reconstruction.

Neural Radiance Fields (NeRF) [Mildenhall et al. 2020] have made groundbreaking strides in rendering complex scenes with remarkable fidelity. Recent advancements have further improved NeRF’s capabilities, such as anti-aliasing [Barron et al. 2021, 2022], handling transient elements [Liu et al. 2023a; Martin-Brualla et al. 2021], and addressing inconsistent camera exposure or illumination [Mildenhall et al. 2020; Rematas et al. 2022]. However, a notable limitation of NeRF lies in its handling of reflections. As illustrated in Figure 2(a), NeRF traces only a single ray and relies on view-dependency or false geometry to account for reflections. For low-frequency reflections like highlights, this is achieved by inputting 3D point positions and viewing directions into a small MLP, which predicts view-dependent emitted radiance. However, this method falls short when dealing with complex, high-frequency reflections. NeRF tends to create false geometry along the primary ray, incorrectly mirroring the actual object’s position along the reflected ray to represent planar reflections (Figure 2a). While this offers a plausible explanation for reflections, it fundamentally misinterprets them. NeRF cannot distinguish a reflected object from a duplicated one, as both appear visually similar. This misrepresentation prevents us from creating correct novel views if we see the space *behind* the reflector, not *through* the reflector. It also leads to incorrect scene geometry, adversely affecting downstream applications, such as mesh extraction.

Several methods have been proposed to address reflections in NeRF [Guo et al. 2022; Liu et al. 2023b; Ma et al. 2024; Verbin et al. 2022, 2024; Yin et al. 2023]. NeRFReN [Guo et al. 2022] proposes to model the transmitted and reflected parts of a forward-facing

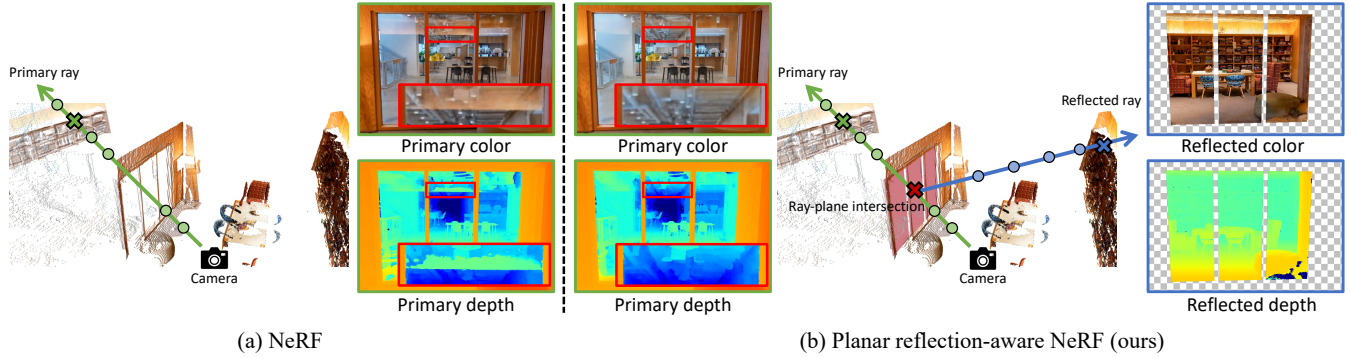


Fig. 2. **Why NeRF generates false geometry?** (a) NeRF only traces a single ray, thus incorrectly interpreting reflections as false geometry, leading to inaccurate scene representations. (b) Our planar reflection-aware NeRF addresses this by employing the law of reflection during rendering, which involves explicitly casting a reflected ray to capture the *source* of the reflections. Our method prevents the creation of false geometries along the primary ray at depths corresponding to real objects on the reflected ray.

scene with separate neural radiance fields. MS-NeRF [Yin et al. 2023] represents the scene using multiple feature fields decoded by small MLPs for rendering and blending. These methods decompose the scene into several *independent* components in a self-supervised manner, sometimes leading to sub-optimal decomposition where false geometries persist in the primary component. Ref-NeRF [Verbin et al. 2022] addresses specular reflections by explicitly parameterizing outgoing radiance as a function of the reflection of the view direction about the local normal vector. It shows promising results in representing specular reflections but lacks the ability to separate reflections.

In this paper, we introduce a planar reflection-aware NeRF that jointly models planar surfaces and explicitly casts reflected rays to capture the *source* of high-frequency reflections (Figure 2 b). Our core idea is to maintain a *single* geometry and appearance instance. This principle dictates that if a real object is present along the reflected ray, our method should not create a false duplicate along the primary ray at the same depth to explain the reflection. Instead, it should always use the reflected ray to explain the reflection, ensuring the primary view is clean and accurate. To render novel views, we query a *single* radiance field to render the primary color and the source of the reflection. Then, we learn to attenuate the source of the reflection and compose it with the primary color to obtain the final color. We introduce regularization to help utilize the true source of reflections for rendering planar reflections rather than creating a false duplicate. As a result, we obtain accurate scene geometry. Rendering along the primary ray results in a clean, reflection-free view, while explicitly rendering along the reflected ray allows us to reconstruct highly detailed reflections. We validate our method’s reconstruction performance on our real-world 360-degree dataset and demonstrate significant enhancements in NeRF’s performance in handling reflections.

Our contributions are summarized as follows:

- We introduce a method for handling planar reflections by jointly modeling planar surfaces and casting reflected rays to accurately capture the source of high-frequency reflections.

- We develop a regularization loss to discourage the creation of false geometries.
- We provide a real-world 360-degree dataset that contains pronounced reflections, facilitating the quantitative evaluation of reflection-free reconstruction.

2 RELATED WORK

Novel view synthesis. Novel view synthesis aims to generate new views from a set of posed images [Chaurasia et al. 2013; Shum and Kang 2000]. Techniques such as light fields [Levoy and Hanrahan 1996] and Lumigraph [Gortler et al. 1996] leverage implicit scene geometry to synthesize realistic appearances, although they require densely captured images. High-quality synthesis with fewer input images is achievable using explicit geometric proxies [Buehler et al. 2001], yet accurately estimating scene geometry remains challenging due to issues like highlights and reflections. Prior work has addressed these challenges through learning-based dense depth maps [Flynn et al. 2016], MPis [Choi et al. 2019; Flynn et al. 2019; Srinivasan et al. 2019], the incorporation of learned deep features [Hedman et al. 2018; Riegler and Koltun 2020], or voxel-based implicit scene representations [Sitzmann et al. 2019], utilizing proxy scene geometry for enhanced rendering. Recently, neural implicit representations, particularly NeRF [Mildenhall et al. 2020], have shown promising results in this domain. However, achieving high-quality, artifact-free rendering remains a substantial challenge. Advancements in NeRF technology, such as anti-aliasing [Barron et al. 2021, 2022, 2023], handling of transient elements [Gao et al. 2021; Li et al. 2021; Liu et al. 2023a; Martin-Brualla et al. 2021], adjustments for inconsistent camera exposure or illumination [Mildenhall et al. 2020; Rematas et al. 2022], and improvements in training efficiency [Chen et al. 2022; Fridovich-Keil et al. 2022; Müller et al. 2022; Sun et al. 2022], have further refined the quality of rendered outputs. While these methods yield high-quality results, a notable limitation lies in their handling of reflections. NeRF is effective for low-frequency reflections but struggles with more complex, high-frequency planar reflections. In this work, we focus on handling planar reflections to facilitate reflection-free novel view synthesis.

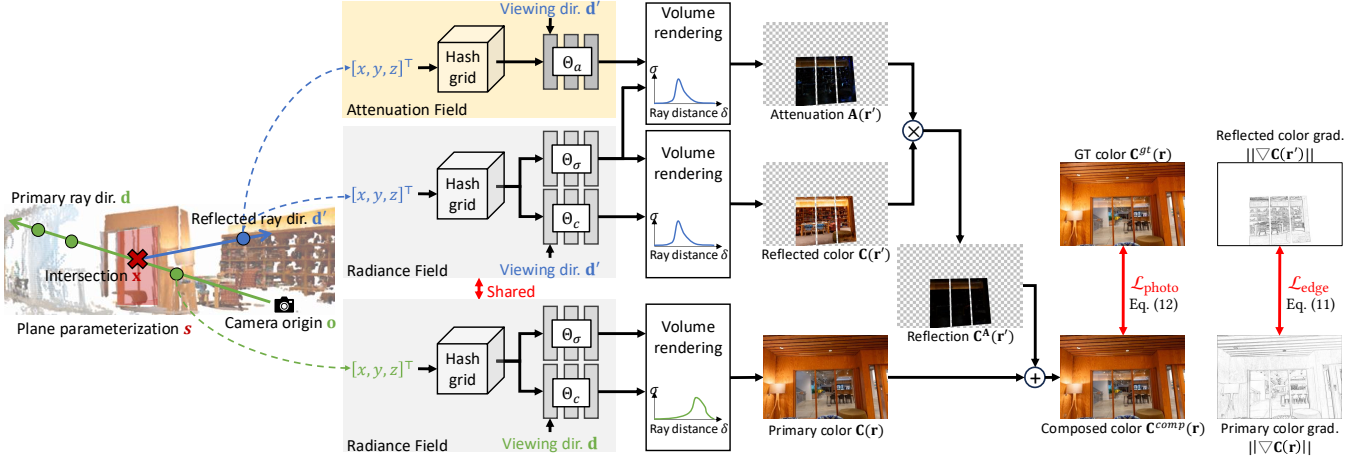


Fig. 3. **Overall framework.** Our method takes a multi-view capture as input. We first detect potential planar reflectors (e.g., window planes). Then for each camera ray, denoted by (\mathbf{o}, \mathbf{d}) where \mathbf{o} is the origin and \mathbf{d} the viewing direction, the 3D coordinates of sampled points and their viewing directions serve as inputs to predict volumetric density σ and color \mathbf{c} . Upon intersecting with a plane, a reflected ray \mathbf{r}' emanates from the point of intersection \mathbf{x} , with its new direction \mathbf{d}' computed as per Eq. (6). This reflected ray probes the same radiance field to obtain the density and color. Through volume rendering, colors $\mathbf{C}(\mathbf{r})$ and $\mathbf{C}(\mathbf{r}')$ are computed for the primary and reflected rays, respectively. To model the Fresnel effect, account for HDR tonemapping, and absorb errors due to intensity clipping, we introduce an attenuation field to adjust the reflected color. We add the reflection $\mathbf{C}^A(\mathbf{r}')$ to the primary color $\mathbf{C}(\mathbf{r})$ to yield the composited color. The reconstruction loss is calculated between the composited color \mathbf{C}^{comp} and the ground truth \mathbf{C}^{gt} . We also apply the sparse edge regularization between the primary color gradient and the reflected color gradient. The loss is backpropagated to update the radiance field, the attenuation field, and the plane parameters.

Reflection modeling. In computer vision and graphics, reflections are a significant challenge. Traditional graphics techniques utilize ray tracing to simulate reflections with high accuracy but at a high computational cost. More recent works have explored incorporating reflection models into neural rendering pipelines, allowing for more efficient and realistic rendering of reflective surfaces. Ref-NeRF [Verbin et al. 2022] addresses specular reflections by explicitly parameterizing outgoing radiance as a function of the reflection of the view direction about the local normal vector. It shows promising results in representing specular reflections but cannot separate reflections. TraM-NeRF [Holland et al. 2023] models mirror-like reflection behavior but overlooks transmission and does not focus on separating reflections. Mirror-NeRF [Zeng et al. 2023] has a similar reflected ray tracing idea to ours but focuses on mirrors. It does not consider transmission and thus is not able to handle transparent reflectors.

Scene decomposition. Recent efforts have attempted to extend NeRF to handle reflections by introducing additional network outputs. NeRFReN [Guo et al. 2022] proposes modeling the transmitted and reflected parts of the forward-facing scene with separate neural radiance fields. The final image is obtained by composing the results from these two radiance fields. MS-NeRF [Yin et al. 2023] represents the scene using multiple feature fields decoded by small MLPs for rendering and blending. These methods decompose the scene into independent components in a self-supervised manner, sometimes leading to suboptimal decomposition where false geometries caused by reflections persist. In contrast, our reflection-aware NeRF employs a *single* radiance field while explicitly casting reflected rays to capture the source of reflections. It adheres to the principle that

if an actual object is observed along the reflected ray, no false duplicate should be created along the primary ray at the same depth. Instead, the reflected ray explains the reflection, ensuring a clean and accurate primary view.

3 METHOD

This section first recapitulates neural radiance fields in Section 3.1. We then provide an overview of our method in Section 3.2. Subsequently, we delve into the details of our reflection-aware NeRF in Section 3.4. We discuss the sparse edge regularization and training strategies in Section 3.5. Finally, we outline the implementation details in Section 3.6.

3.1 Neural Radiance Fields

Neural Radiance Fields (NeRF) [Mildenhall et al. 2020] employ MLPs parameterized by Θ to map the 3D position $\mathbf{x} = (x, y, z)$ and the normalized viewing direction $\mathbf{d} = (d_x, d_y, d_z) \in \mathbb{R}^3$ to the corresponding volume density σ and color \mathbf{c} .

$$(\sigma, \mathbf{c}) = \text{MLP}_{\Theta}(\mathbf{x}, \mathbf{d}). \quad (1)$$

The color of a pixel can be computed by performing volume rendering along the ray \mathbf{r} , emitted from the camera origin [Drebin et al. 1988]:

$$\mathbf{C}(\mathbf{r}) = \sum_{k=1}^K T_k \left(1 - e^{-\sigma_k \delta_k}\right) \mathbf{c}_k, \quad (2)$$

$$T_k = e^{-\sum_{k'=1}^{k-1} \sigma_{k'} \delta_{k'}}, \quad (3)$$

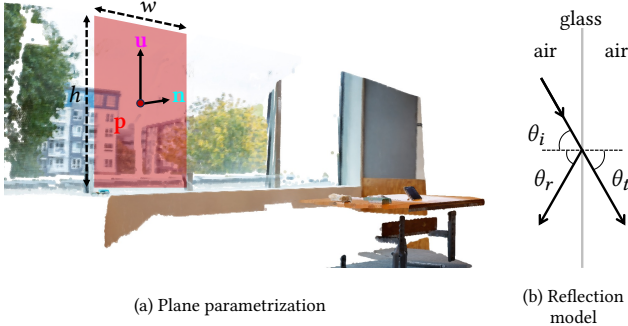


Fig. 4. **Reflection model.** (a) Our plane is parameterized by a center \mathbf{p} , a normal \mathbf{n} , an up vector \mathbf{u} , and width and height (w, h). (b) We adopt a simple reflection model to conceptualize the reflection process as involving solely a primary incident ray and its consequent reflected ray, effectively neglecting any refraction effects that would arise from a finite glass thickness.

where $\delta(k)$ is the distance between two consecutive points along the ray, K denotes the number of samples along each ray, and T_k indicates the accumulated transmittance.

To optimize the weights Θ of the NeRF model, we first construct the camera ray $\mathbf{r} = (\mathbf{o}, \mathbf{d})$, where \mathbf{o} is the camera origin and \mathbf{d} is the viewing direction. We can then optimize Θ_s by minimizing the photometric loss between the rendered color \mathbf{C} and the ground truth color \mathbf{C}^{gt} :

$$\mathcal{L} = \|\mathbf{C}(\mathbf{r}) - \mathbf{C}^{gt}(\mathbf{r})\|_2^2. \quad (4)$$

3.2 Method Overview

We show our proposed framework in Figure 3. We tackle the challenging problem of accurately modeling planar reflections. NeRF only traces a single ray, thus tends to create false geometry along the primary ray, incorrectly mirroring the actual object’s position along the reflected ray to represent planar reflections. Figure 2 (a) illustrates this common pitfall with the reflection of a shelf erroneously modeled as a solid object. Thus, in this paper, we introduce a reflection-aware NeRF that jointly models planar surfaces and explicitly casts reflected rays to capture the *source* of the high-frequency reflections (Figure 2 b). Given a multi-view capture of a scene as input, we aim to improve the rendering quality in the reflection regions and obtain accurate geometry.

3.3 Plane Annotation and Parameterization

We propose a simple method to detect and annotate planes. We first train an InstantNGP and render the depth maps. We use Segment Anything (SAM) [Ma et al. 2024] to segment the windows in 2D and unproject the four dilated corners into 3D space using the depth map. A least square fit to these points gives us a plane parameter initialization. Following NeurMiPs [Lin et al. 2022], a plane segment is parameterized by $\mathbf{s} = (\mathbf{p}, \mathbf{n}, \mathbf{u}, w, h)$, where \mathbf{p} is the plane center; \mathbf{n} is the plane normal; \mathbf{u} is the normalized up vector defining the y-axis direction of the plane; and (w, h) are the dimensions of the plane. See Figure 4 (a) for an illustration of the plane parameterization. Our



Fig. 5. **Plane refinement.** With jointly optimization, our rendered reflection aligns with the observations.

model does not require accurate annotation; these coarsely annotated planes serve as initialization, and the plane parameterization is jointly refined during training (Figure 5).

3.4 Reflection-aware NeRF

Our reflection model. We illustrate our reflection model in Figure 4(b). Applying Snell’s Law at each interface, the outgoing angle of refraction θ_t equals the incoming angle of incidence θ_i . We adopt the following assumptions: 1) the glass is impurity-free and does not scatter light diffusely; 2) the glass is infinitely thin. Based on these assumptions, our model simplifies by considering only the primary and reflected incident ray. The primary ray remains unaltered in its path.

Ray-plane intersection. Given a plane \mathbf{s} and a primary ray (\mathbf{o}, \mathbf{d}) , we can determine whether the ray intersects the plane. First, we find the intersection point \mathbf{x} between the infinite plane (\mathbf{p}, \mathbf{n}) and the ray:

$$\mathbf{x} = \mathbf{o} + t \cdot \mathbf{d}, \quad t = \frac{(\mathbf{p} - \mathbf{o}) \cdot \mathbf{n}}{\mathbf{d} \cdot \mathbf{n}}. \quad (5)$$

We discard rays if the plane is behind the ray’s origin (i.e., when $t < 0$). Additionally, we discard rays whose intersection points do not lie within the finite plane segment. When a ray intersects multiple planes, we select the intersection with the nearest plane.

Casting reflected ray. If a ray intersects a plane, we cast a reflected ray. The new origin of the reflected ray is \mathbf{x} , and the new viewing direction is given by:

$$\mathbf{d}' = \mathbf{d} - 2(\mathbf{d} \cdot \mathbf{n}) \cdot \mathbf{n}. \quad (6)$$

We query the same NeRF model to obtain the volume density σ and color \mathbf{c} for the 3D points along the reflected ray $\mathbf{r}' = (\mathbf{x}, \mathbf{d}')$. Now, if a ray intersects the plane, we can perform volume rendering along each ray to obtain the primary color $\mathbf{C}(\mathbf{r})$ and the source of reflection $\mathbf{C}(\mathbf{r}')$. Next, we discuss how we compose these two components to calculate the final color.

Composing primary and reflected ray. We introduce a dual-function attenuation field to model both actual attenuation (such as Fresnel effects) and compositing, diverging from conventional physics-based models that rely solely on Fresnel equations to determine reflection and transmission coefficients based on the viewing direction. Fresnel equations rely on the assumption of a linear color space. However, following tone mapping, RGB values no longer reside in a linear space, thus invalidating the direct application of the Fresnel equation. Therefore, we propose optimizing an adaptable

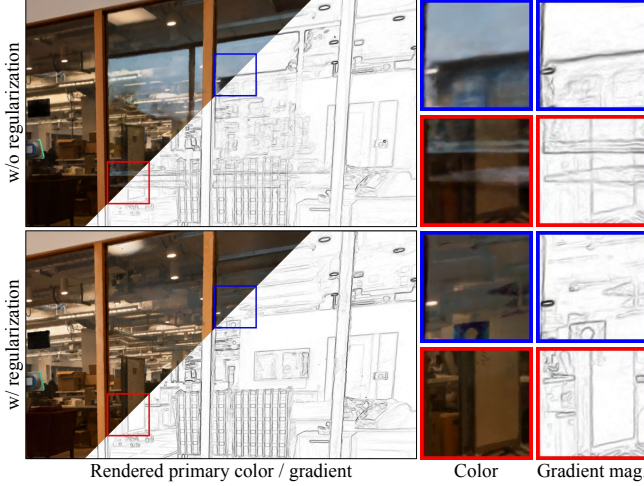


Fig. 6. **Sparse edge regularization.** By applying the sparse edge regularization, the primary view is clean and free of false geometries.

attenuation field that compensates for the non-linearity introduced by HDR tone mapping, models the Fresnel effect, and absorbs errors due to intensity clipping. Since attenuation is associated with the intensity of the reflection, our attenuation field maps the 3D position (x, y, z) along the reflected ray \mathbf{r}' and the normalized reflected viewing direction \mathbf{d}' to the corresponding attenuation a , rather than using the primary ray to predict the attenuation as previous work did [Guo et al. 2022]:

$$a = \text{MLP}_a(x, y, z, \mathbf{d}') \quad (7)$$

$$\mathbf{A}(\mathbf{r}') = \sum_{k=1}^K T_k \left(1 - e^{-\sigma_k \delta_k}\right) a_k \quad (8)$$

To calculate the final color, we additionally obtain the transmittance T of each ray at the intersection using Eq. (3). The final color is composited by:

$$\mathbf{C}^{\text{comp}}(\mathbf{r}) = \mathbf{C}(\mathbf{r}) + T \cdot \mathbf{C}^{\mathbf{A}}(\mathbf{r}'), \quad (9)$$

where the attenuated reflection is calculated by

$$\mathbf{C}^{\mathbf{A}}(\mathbf{r}') = \sum_{k=1}^K T_k \left(1 - e^{-\sigma_k \delta_k}\right) (a_k \cdot c_k) \quad (10)$$

We demonstrate in the experimental section that our attenuation field consistently learns attenuation with robustness in real-world scenarios.

3.5 Training

Training our reflection-aware NeRF requires jointly optimizing the plane geometry \mathbf{s} , the radiance field, and the attenuation field. In the following, we discuss two key training strategies: 1) sparse edge regularization; 2) scheduling.

Sparse edge regularization. Even with our proposed reflection model, the network still tends to reject the model by learning a small attenuation number. It has a propensity to introduce false geometry along the primary ray $\mathbf{C}(\mathbf{r})$, situated at the same depth as

Table 1. **Quantitative evaluation on reflection removal.** We report the average PSNR, SSIM and LPIPS results with comparisons to existing methods on the held-out reflection-free views captured *outside* the rooms.

	PSNR \uparrow	SSIM \uparrow	LPIPS \downarrow
NeRFReN [Guo et al. 2022]	12.27	0.3786	0.760
MS-NeRF [Yin et al. 2023]	13.28	0.4580	0.657
Ours	15.04	0.5885	0.446

the actual object along the reflected ray $\mathbf{C}(\mathbf{r}')$. To mitigate this issue of duplication, we leverage a sparse edge regularization. Utilizing the Sobel operator ∇ , we compute the gradients to identify edges within the image. Sparse edge regularization is applied by minimizing element-wise multiplication between the gradient of the primary colors and those of the reflected colors:

$$\mathcal{L}_{\text{edge}} = \|\nabla(\mathbf{C}(\mathbf{r})) * \nabla(\mathbf{C}(\mathbf{r}'))\|_1. \quad (11)$$

We detach the gradient flow from $\mathcal{L}_{\text{edge}}$ to $\mathbf{C}(\mathbf{r}')$ to constrain the regularization strictly to the primary colors. The underlying principle is that if an edge is discernible in the reflected color image (indicative of the source of reflection), such an edge should not concurrently exist in the primary color image. This regularization effectively prevents the primary color from incorporating duplicated objects, as shown in Figure 6.

Training scheduling. We first initialize the plane geometric parameters \mathbf{s} using the annotation. Then, we jointly optimize the plane geometry \mathbf{s} , the radiance field, and the attenuation field using photometric loss:

$$\mathcal{L}_{\text{photo}} = \|\mathbf{C}^{\text{comp}}(\mathbf{r}) - \mathbf{C}^{\text{gt}}(\mathbf{r})\|_2^2. \quad (12)$$

We show in Figure 5 that with joint optimization, our rendered reflection aligns perfectly with the observations. Upon reaching the 50K iteration, we cease adjustments to \mathbf{s} and proceed to refine the model with the sparse edge regularization loss for an additional 50K iterations:

$$\mathcal{L} = \mathcal{L}_{\text{photo}} + 0.5\mathcal{L}_{\text{edge}}. \quad (13)$$

The sparse edge regularization helps eliminate false geometries but also diminishes the reconstruction sharpness. We fix the attenuation field to restore detail and gradually decay the weight for sparse edge regularization for another 100K iterations.

3.6 Implementation Details

We implement our approach using a single NVIDIA V100 GPU. We use one set of hyperparameters for all experiments. Our network follows the default InstantNGP design (hash grid + MLP) to predict color and density and uses an additional NGP to predict the attenuation. We parameterize the scenes using the contraction parameterization [Barron et al. 2022]. Compared to the vanilla InstantNGP framework which requires 5 hours to complete 150k iterations, our RA-NeRF requires only an additional 2 hours to complete the same number of iterations.

4 EXPERIMENTAL RESULTS

4.1 Dataset

To address the scarcity of real-world 360-degree datasets that contain pronounced reflections, we present the *Office dataset*. This dataset

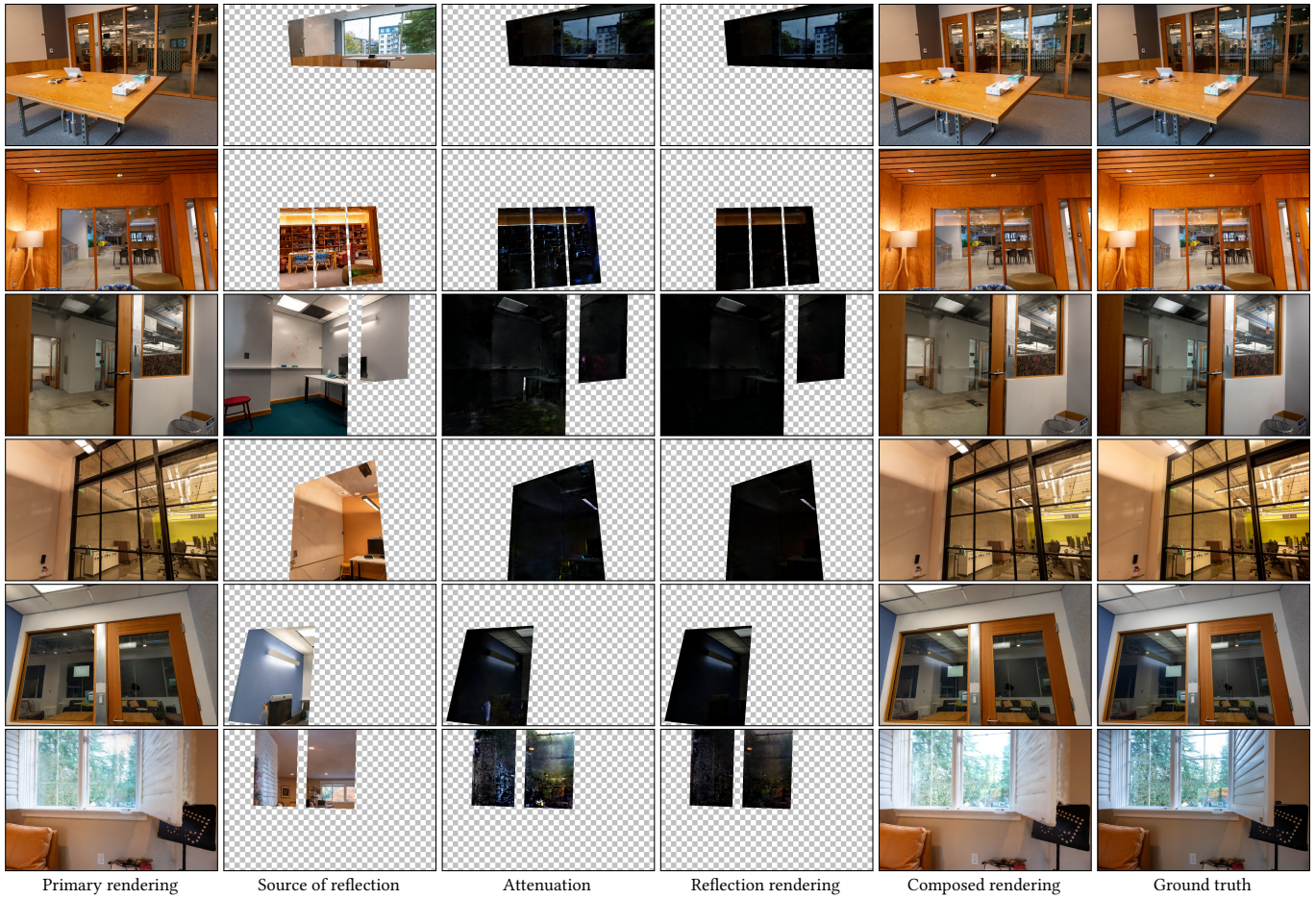


Fig. 7. **Individual component.** Rendering along the primary ray yields a reflection-free image. Rendering along the reflected ray captures the source of the reflection. The final image is composed by combining the reflection-free image with the attenuated source of the reflection. Our method ensures that reflections are effectively isolated and can be manipulated independently from the reflection-free scene reconstruction.

contains six distinct 360-degree scenes captured in office environments where reflections are prominently caused by window glass. We capture each scene from both interior and exterior perspectives. The dataset is organized into three splits: *inside-train*, *inside-val*, and *outside*. The *inside-train* and *inside-val* splits feature images with reflections, while the *outside* split consists of images without reflections.

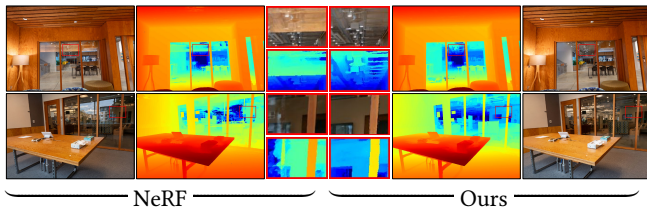


Fig. 8. **Accurate geometry.** By explicitly casting reflected rays, our method ensures accurate geometry representation, which is not degraded by the false geometries introduced by reflections.



Fig. 9. **Reflection-removal comparison on the outside split.** We evaluate the reflection-removal performance of each method using held-out views captured *outside* the rooms. As the query viewpoints outside the room are far from the training views (inside the room), artifacts are thus visible.

Table 2. **Quantitative evaluation on reconstruction.** We report the average PSNR, SSIM and LPIPS results with comparisons to existing methods on Office dataset *inside-val* split. The best performance is in **bold** and the second best is underscored.

PSNR ↑ / SSIM ↑ / LPIPS ↓	Game Room	Meeting Room 1	Meeting Room 2	Meeting Room 3	Meeting Room 4	Home Office	Average
NeRFReN [Guo et al. 2022]	17.81 / 0.5035 / 0.337	19.76 / 0.5871 / 0.431	22.67 / 0.8497 / 0.218	21.30 / 0.8072 / 0.253	24.96 / 0.8660 / 0.222	14.78 / 0.4465 / 0.592	20.43 / 0.6924 / 0.343
MS-NeRF [Yin et al. 2023]	<u>23.68</u> / <u>0.8281</u> / <u>0.173</u>	28.21 / 0.8450 / 0.196	<u>24.54</u> / <u>0.8688</u> / <u>0.189</u>	24.91 / 0.8439 / 0.213	22.18 / 0.7940 / 0.342	15.89 / 0.6396 / 0.454	23.20 / 0.8010 / 0.269
Ref-NeRF [Verbin et al. 2022]	22.46 / 0.7152 / 0.318	<u>25.86</u> / <u>0.7572</u> / <u>0.307</u>	22.30 / 0.7599 / 0.389	<u>23.28</u> / <u>0.7205</u> / <u>0.365</u>	24.20 / 0.8054 / 0.314	<u>16.26</u> / 0.5466 / 0.710	22.39 / 0.7177 / 0.408
Ours	24.45 / 0.9140 / 0.076	23.14 / 0.8847 / 0.125	24.69 / 0.9218 / 0.132	21.99 / 0.9106 / 0.096	<u>24.66</u> / 0.9351 / 0.109	17.47 / 0.8196 / 0.232	<u>22.58</u> / 0.8962 / 0.133

4.2 Experimental setup

Our evaluation focuses on two key scenarios: 1) reflection-free reconstruction and 2) improved rendering quality (with reflection). For evaluating reflection-free reconstruction, we train our model on the *inside-train* split and test on the *outside* split. For evaluating improved rendering quality, we train on the *inside-train* split and validate on the *inside-val* split.

Reflection-free reconstruction. We qualitatively assess the capacity of our reflection-aware NeRF for reflection-free reconstruction using the *inside-val* split in Figure 7. This process involves rendering along the primary ray to produce a reflection-free image and along the reflected ray to capture the source of the reflection. The final image is composed by blending these two images using the predicted attenuation and plane intersection transmittance as in Eq. (9). The results demonstrate our method’s capability in synthesizing *reflection-free* views. We show in Figure 8 that this leads to more accurate scene geometry reconstruction. We also compare our method’s reflection removal performance against NeRFReN [Guo et al. 2022] and MS-NeRF [Yin et al. 2023] on the held-out *outside* views in Table 1 and Figure 9. However, as the query viewpoints outside the room are far from the training views (inside the room), artifacts are therefore visible. Therefore, we also conduct a qualitative comparison on the held-out *inside-val* views in Figure 10 (no reflection-free ground truth is available). We used the official code of MS-NeRF for scene decomposition. Since the decomposition is unsupervised, we had to manually select the most suitable decoded images to represent the reflection-free results. NeRFReN was designed for forward-facing scenes. To train a NeRFReN model, we constructed a subset of *inside-train*, which only contains forward-facing views.

Improved rendering quality. We benchmark the reconstruction quality of our method against several baseline methods. The comparisons are detailed in Table 2 and Figure 13. Our method, with its explicit modeling of reflections, achieves results with sharper reflections and noticeably fewer artifacts. Although our results are much sharper and achieve better scores on SSIM and LPIPS, they are darker due to attenuation, which significantly impacts pixel-wise metrics like PSNR.

4.3 Non-transparent Plane

Our method can handle more than just transparent planes; it can also process opaque surfaces. We demonstrate our method on an opaque countertop in Figure 11.



Fig. 10. **Reflection-removal comparison on the inside-val split.** We qualitatively evaluate the reflection-removal performance of each method using held-out views captured *inside* the rooms.

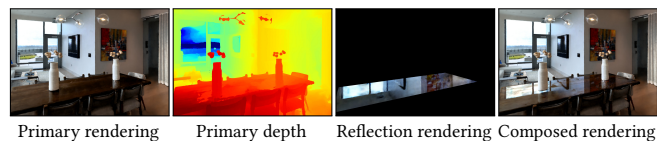


Fig. 11. **Non-transparent Plane.** We showcase our method’s ability to handle non-transparent planes.

4.4 Ablation Study

We quantitatively ablate each key component on challenging held-out *outside* views that deviate significantly from the training views in Table 3. The joint refinement of planes is a critical component of our framework. As illustrated in Figure 5, there is a noticeable spatial misalignment between the rendered reflection and the observed image prior to refinement. Joint optimization resolves this issue, achieving better alignment between our rendered reflections and the observed images. Our sparse edge regularization is critical in preventing the duplication of objects. Without this regularization, as shown in Figure 6, the network tends to introduce false geometry along the primary ray, situated at the same depth as the actual object along the reflected ray. Our regularization approach effectively mitigates this issue. Note that the margin appears relatively small because the overall number is lower due to significant view extrapolation. The implementation of training scheduling enhances the visual quality of the results. This approach fine-tunes the training process, leading to more refined and visually appealing results.

Table 3. **Ablation study.** We report PSNR, SSIM and LPIPS on the Game Room sequence.

	PSNR \uparrow	SSIM \uparrow	LPIPS \downarrow
Ours w/o jointly plane refinement	19.38	0.8123	0.138
Ours w/o training scheduling	20.01	0.7924	0.154
Ours w/o \mathcal{L}_{edge}	20.18	0.8144	0.141
Ours	20.28	0.8216	0.129

Fig. 12. **Failure cases.** (a) Despite the implementation of sparse edge regularization, our method may be less effective for textureless, edge-blurry reflections. (b) Inaccuracies in predicted attenuation, especially for high-lights, result in erroneous illumination effects.

4.5 Limitations

In this paper, we focus on glass-material planar reflectors (e.g., windows) because they are ubiquitous in indoor scenes and challenging to model with existing radiance fields. We assume perfect planar reflection and do not model nonlinear distortion. We acknowledge that a highly curved surface or an imperfect surface may invalidate our assumptions and lead to degradation in performance. We plan to address these in future work. In Figure 12, we present some instances where our approach did not yield the desired results. Our method may be less effective in textureless regions, edge-blurry areas, and regions with highlights.

REFERENCES

Jonathan T Barron, Ben Mildenhall, Matthew Tancik, Peter Hedman, Ricardo Martin-Brualla, and Pratul P Srinivasan. 2021. Mip-nerf: A multiscale representation for anti-aliasing neural radiance fields. In *ICCV*.

Jonathan T Barron, Ben Mildenhall, Dor Verbin, Pratul P Srinivasan, and Peter Hedman. 2022. Mip-nerf 360: Unbounded anti-aliased neural radiance fields. In *CVPR*.

Jonathan T Barron, Ben Mildenhall, Dor Verbin, Pratul P Srinivasan, and Peter Hedman. 2023. Zip-nerf: Anti-aliased grid-based neural radiance fields. In *Proceedings of the IEEE/CVF International Conference on Computer Vision*. 19697–19705.

Chris Buehler, Michael Bosse, Leonard McMillan, Steven Gortler, and Michael Cohen. 2001. Unstructured lumigraph rendering. In *Proceedings of the 28th annual conference on Computer graphics and interactive techniques*. 425–432.

Gaurav Chaurasia, Sylvain Duchene, Olga Sorkine-Hornung, and George Drettakis. 2013. Depth synthesis and local warps for plausible image-based navigation. *ACM TOG* 32 (2013), 1–12.

Anpei Chen, Zexiang Xu, Andreas Geiger, Jingyi Yu, and Hao Su. 2022. TensorRF: Tensorial Radiance Fields. In *ECCV*.

Inchang Choi, Orazio Gallo, Alejandro Troccoli, Min H Kim, and Jan Kautz. 2019. Extreme view synthesis. In *ICCV*.

Robert A Drebin, Loren Carpenter, and Pat Hanrahan. 1988. Volume rendering. *ACM TOG* 22 (1988), 65–74.

John Flynn, Michael Broxton, Paul Debevec, Matthew DuVall, Graham Fyffe, Ryan Overbeck, Noah Snavely, and Richard Tucker. 2019. Deepview: View synthesis with learned gradient descent. In *CVPR*.

John Flynn, Ivan Neulander, James Philbin, and Noah Snavely. 2016. Deepstereo: Learning to predict new views from the world’s imagery. In *CVPR*.

Sara Fridovich-Keil, Alex Yu, Matthew Tancik, Qinzhong Chen, Benjamin Recht, and Angjoo Kanazawa. 2022. Plenoxels: Radiance Fields Without Neural Networks. In

CVPR.

Chen Gao, Ayush Saraf, Johannes Kopf, and Jia-Bin Huang. 2021. Dynamic view synthesis from dynamic monocular video. In *ICCV*.

Steven J Gortler, Radek Grzeszczuk, Richard Szeliski, and Michael F Cohen. 1996. The lumigraph. In *Proceedings of the 23rd annual conference on Computer graphics and interactive techniques*. 43–54.

Yuan-Chen Guo, Di Kang, Linchao Bao, Yu He, and Song-Hai Zhang. 2022. NeRFNe: Neural Radiance Fields With Reflections. In *CVPR*.

Peter Hedman, Julien Philip, True Price, Jan-Michael Frahm, George Drettakis, and Gabriel Brostow. 2018. Deep blending for free-viewpoint image-based rendering. *ACM TOG* 37 (2018), 1–15.

Leif Van Holland, Ruben Bliersbach, Jan U Müller, Patrick Stotko, and Reinhard Klein. 2023. TraM-NeRF: Tracing Mirror and Near-Perfect Specular Reflections Through Neural Radiance Fields. In *Computer Graphics Forum*, e15163.

Marc Levoy and Pat Hanrahan. 1996. Light field rendering. In *Proceedings of the 23rd annual conference on Computer graphics and interactive techniques*. 31–42.

Zhengqi Li, Simon Niklaus, Noah Snavely, and Oliver Wang. 2021. Neural scene flow fields for space-time view synthesis of dynamic scenes. In *CVPR*.

Zhi-Hao Lin, Wei-Chiu Ma, Hao-Yu Hsu, Yu-Chiang Frank Wang, and Shenlong Wang. 2022. Neurmips: Neural mixture of planar experts for view synthesis. In *CVPR*.

Yuan Liu, Peng Wang, Cheng Lin, Xiaoxiao Long, Jiepeng Wang, Lingjie Liu, Taku Komura, and Wenping Wang. 2023b. Nero: Neural geometry and brdf reconstruction of reflective objects from multiview images. *ACM Transactions on Graphics (TOG)* 42, 4 (2023), 1–22.

Yu-Lun Liu, Chen Gao, Andreas Meuleman, Hung-Yu Tseng, Ayush Saraf, Changil Kim, Yung-Yu Chuang, Johannes Kopf, and Jia-Bin Huang. 2023a. Robust Dynamic Radiance Fields. In *Proceedings of the IEEE/CVF Conference on Computer Vision and Pattern Recognition*.

Li Ma, Vasu Agrawal, Haithem Turki, Changil Kim, Chen Gao, Pedro Sander, Michael Zollhöfer, and Christian Richardt. 2024. SpecNeRF: Gaussian Directional Encoding for Specular Reflections. In *Proceedings of the IEEE/CVF International Conference on Computer Vision*.

Ricardo Martin-Brualla, Noha Radwan, Mehdi SM Sajjadi, Jonathan T Barron, Alexey Dosovitskiy, and Daniel Duckworth. 2021. Nerf in the wild: Neural radiance fields for unconstrained photo collections. In *CVPR*.

Ben Mildenhall, Pratul P. Srinivasan, Matthew Tancik, Jonathan T. Barron, Ravi Ramamoorthi, and Ren Ng. 2020. NeRF: Representing Scenes as Neural Radiance Fields for View Synthesis. In *ECCV*.

Thomas Müller, Alex Evans, Christoph Schied, and Alexander Keller. 2022. Instant neural graphics primitives with a multiresolution hash encoding. *ACM TOG* 41 (2022), 102:1–102:15.

Konstantinos Rematas, Andrew Liu, Pratul P. Srinivasan, Jonathan T. Barron, Andrea Tagliasacchi, Tom Funkhouser, and Vittorio Ferrari. 2022. Urban Radiance Fields. In *CVPR*.

Gernot Riegler and Vladlen Koltun. 2020. Free view synthesis. In *ECCV*.

Harry Shum and Sing Bing Kang. 2000. Review of image-based rendering techniques. In *Visual Communications and Image Processing 2000*, Vol. 4067. 2–13.

Vincent Sitzmann, Michael Zollhöfer, and Gordon Wetzstein. 2019. Scene representation networks: Continuous 3d-structure-aware neural scene representations. In *NeurIPS*.

Pratul P Srinivasan, Richard Tucker, Jonathan T Barron, Ravi Ramamoorthi, Ren Ng, and Noah Snavely. 2019. Pushing the boundaries of view extrapolation with multiplane images. In *CVPR*.

Cheng Sun, Min Sun, and Hwann-Tzong Chen. 2022. Direct voxel grid optimization: Super-fast convergence for radiance fields reconstruction. In *CVPR*.

Dor Verbin, Peter Hedman, Ben Mildenhall, Todd Zickler, Jonathan T. Barron, and Pratul P. Srinivasan. 2022. Ref-NeRF: Structured View-Dependent Appearance for Neural Radiance Fields. In *CVPR*.

Dor Verbin, Pratul P Srinivasan, Peter Hedman, Ben Mildenhall, Benjamin Attal, Richard Szeliski, and Jonathan T Barron. 2024. NeRF-Casting: Improved View-Dependent Appearance with Consistent Reflections. *arXiv preprint arXiv:2405.14871* (2024).

Ze-Xin Yin, Jiaxiang Qiu, Ming-Ming Cheng, and Bo Ren. 2023. Multi-Space Neural Radiance Fields. In *CVPR*.

Junyi Zeng, Chong Bao, Rui Chen, Zilong Dong, Guofeng Zhang, Hujun Bao, and Zhaopeng Cui. 2023. Mirror-NeRF: Learning Neural Radiance Fields for Mirrors with Whitted-Style Ray Tracing. In *Proceedings of the 31st ACM International Conference on Multimedia*.

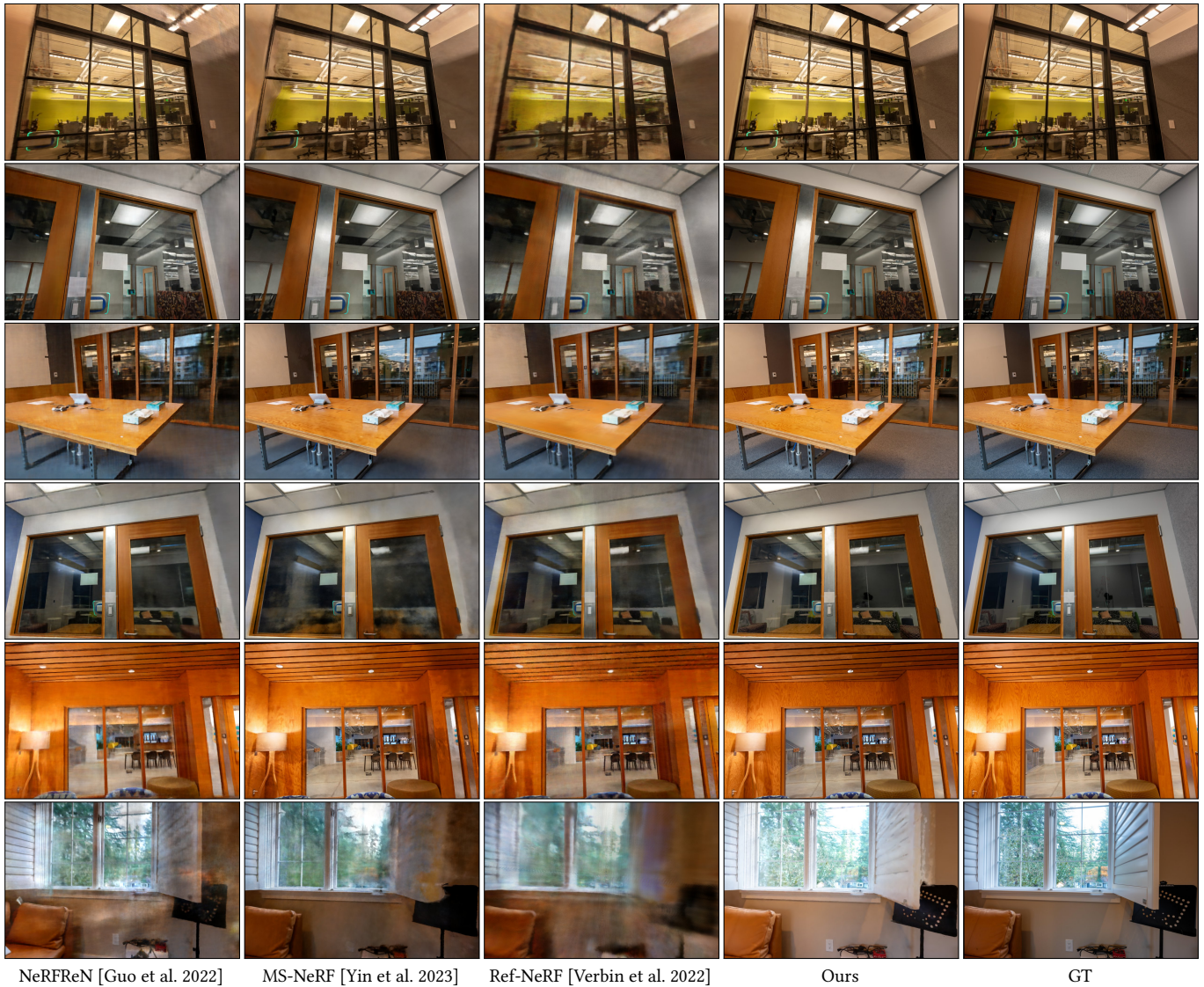


Fig. 13. **Reconstruction comparisons.** Owing to our method’s explicit modeling of reflections, our results exhibit sharper reflections with fewer artifacts compared to other methods.